

Electronic Supplementary Information for: *Unbiased,
complete solar charging of a neutral flow battery by a single
Si photocathode*

Kristina Wedege^a, Dowon Bae^b, Emil Dražević^a, Adélio Mendes^c, Peter C.K.
Vesborg^{*b} and Anders Bentien^{*a}

^a*Department of Engineering, Aarhus University, Hångøvej 2, DK-8200 Aarhus, Denmark*

^b*Department of Physics, Technical University of Denmark, DK-2800 Kgs. Lyngby, Denmark*

^c*LEPABE - Department of Chemical Engineering, University of Porto, Rua Dr. Roberto Frias S/N P-4200-465, Porto,
Portugal*

S1: Notes for literature review (Figure 1)

In Figure 1 of the main paper, the following abbreviations are used: AQDS = anthraquinone-2,7-disulfonate, DSSC = dye sensitized solar cell, BQDS = 4,5-dihydroxy-1,3-benzenedisulfonate, AQS = anthraquinone-2-sulfonate, DHAQ = 2,6-dihydroxyanthraquinone.

The limiting electrolyte energy density used here is calculated by multiplying the concentration of the least soluble redox specie with the numbers of electrons involved in its redox reaction, the Faraday constant and the cell voltage. We calculate this quantity in order to reach comparable numbers (given the variety of flow battery electrolyte concentrations chosen in the references for Figure 1 in the main paper by different researchers), but note that both electrolyte reservoirs should ideally be taking into account resulting in a full energy density that is half of that reported here, if the redox species concentrations were exactly balanced.

In order to compare the maximum solar conversion efficiency for a range of published solar batteries with different characterization strategies, we use the simple efficiency calculation suggested by McKone and coworkers:¹

$$\eta = \frac{\Delta E_{cell} \cdot J_{photo}}{P_{in}}$$

where ΔE_{cell} is the full cell potential (open circuit potential of the battery at the indicated SOC), J_{photo} is the measured photocurrent in mA cm^{-2} and P_{in} is the solar incident power density equal to 100 mW cm^{-2} for 1 sun.

The demonstrated achievable SOC is primarily evaluated from the achievable open-circuit potential upon solar charging the systems and the expected battery potential behaviour with SOC from the Nernst equation as described in the notes below for each paper.

1) In the report *All-vanadium redox photoelectrochemical cell: An approach to store solar energy*,² a TiO_2 photoanode is used to charge 0.01 M solutions of vanadium electrolytes resulting in a cell potential of 1.26 V and the RFB capacity is therefore 0.34 WhL^{-1} . 0.25 mA photocurrent is observed in Figure 4a in the beginning of the solar charging test, and the TiO_2 electrode area is 6.45 cm^2 which gives 0.037 mA cm^{-2} at 0% SOC at a cell potential of 0.68 V giving a solar conversion efficiency of 0.026%. The current decreases to 0.08 mA after 25 h at which the authors assume that the cell is 6 % charged from absorbance measurements, though the cell potential reached is only 0.78 V which would correspond to a only slightly charged battery. Assuming that the cell is actually charged to 6%, the cell potential should be 1.12 V (at which the 25 h solar conversion efficiency would then be 0.01%). Nevertheless, the 6% value is used in Figure 1.

2) In the report *Unbiased solar energy storage: Photoelectrochemical redox flow battery*³ a CdS photoanode is used to charge 0.4 M solutions of vanadium electrolyte, but in the low-voltage configuration where the resulting cell potential is 0.6 V and the RFB capacity is therefore 6.43 WhL^{-1} . Linear sweep voltammograms are shown for different SOC in Figure 4a and it works unbiased up to 75%. The photocurrent at 0 V (no bias) at 25% SOC is 0.4 mA cm^{-2} which gives solar conversion efficiency of 0.2% since the cell voltage is 0.541 V. A sample delivering 1.4 mA cm^{-2} is demonstrated at 0% SOC and assuming a 10 % drop in photocurrent for this sample in going to 25% SOC, the solar conversion efficiency is 0.68% which is the value used in Figure 1. We note that the photoelectrode stability demonstrated is on the minute scale.

3) In the report *Integrating a dual-silicon photoelectrochemical cell into a redox flow battery for unassisted photocharging*⁴ a $\text{pn}^+\text{Si/Ti/TiO}_2/\text{Carbon}$ photocathode and $\text{np}^+\text{Si/Pt}$ photoanode is used to charge either side of a bromine/anthraquinone-2,7-disulfonate RFB where AQDS (2-electron transfer molecule) is used with the capacity limiting concentration of 0.05 M. The theoretical cell potential for this RFB is 0.89 V which then gives a RFB capacity of 2.39 WhL^{-1} . In Figure 6, the photocurrent is approximately 7.4 mA cm^{-2} from the beginning to 1/4 charging time and 6 mA cm^{-2} is reached in the end at which the cell potential had increased to 0.8 V corresponding to 8.6 % SOC. Taking the maximum efficiency at 1/4 charging time using the potential 0.744 V gives a maximum solar conversion efficiency of 5.5 %.

4) In the report *Direct Solar Charging of an Organic-Inorganic, Stable, and Aqueous Alkaline Redox Flow Battery with a Hematite Photoanode*⁵ a hematite-polyaniline photoanode is used in a 0.2 M/0.1 M ferrocyanide/anthraquinone-2,7-disulfonate alkaline RFB with a cell potential of 0.74 V resulting in a RFB capacity of 3.97 WhL^{-1} . Linear sweep voltammograms are shown at different SOC in Figure 4, and

a maximum achievable SOC of 12% is determined from a semi-logarithmic fit of onset potential from LSV solar RFB curves. The maximum conversion efficiency in the cell is determined to be 0.08% in Supporting Information S5.1.

5) In the report *pH-Tuning a Solar Redox Flow Battery for Integrated Energy Conversion and Storage*⁶ a dye-sensitized solar cell (TiO₂ and ruthenium-based dye) is used in a iodide/anthraquinone-2,7-disulfonate RFB from pH 2-8. The AQDS concentration is 0.05 M and the cell potential of 0.46 V at pH 2.9 (optimised value) thus results in RFB capacity of 1.23 WhL⁻¹. The solar charging curve in Figure 4 goes to 0.34 V, which is 3.5% SOC according to the theoretical charging curve. The current goes from 2 to 1.2 mA during the first charging for a 0.424 cm² electrode, so the end solar conversion efficiency is 0.96%, which is similar to the efficiency obtained by calculating halfway through the first cycle at 0.3 V at current 1.4 mA (0.99 %) which is used in Figure 1.

6) In the report *Integrated Photoelectrochemical Solar Energy Conversion and Organic Redox Flow Battery Device*⁷ two Si photoelectrodes (p⁺nn⁺Si/Ti/TiO₂/Pt and n⁺np⁺Si/Ti/TiO₂/Pt) similar to those of reference⁴ are used to charge a 4,5-dihydroxy-1,3-benzenedisulfonate/anthraquinone-2,7-disulfonate RFB. 0.1 M solutions are used, but the cell voltage realised in RFB charging tests are lower than that expected, which warrants a comment here as it significantly changes our determination of the achievable SOC. In the RFB charging/discharging curves of Figure 2a, the cell voltage at 50% SOC can be read off to be not 0.68 V as would be expected from the electrolyte redox potentials, but closer to 0.45 V, as also indicated by the authors in Figure 2b, inset. This is in contrast to the expected behaviour, but nevertheless what the battery tests shows, and thus we use the cell voltage of 0.45 V in calculating energy density to 2.41 WhL⁻¹. Regarding solar conversion efficiency, long-term test (Supporting Information Figure S3) indicate that a potential of 0.53 V can be reached and referring this to the authors' own correlation of SOC and cell voltage, it is seen that around 85% SOC is achievable unbiased. The photocurrent is 20.5 mA cm⁻² at 0.42 V, which gives a solar conversion efficiency of 8.6 %.

7) In the report *Solar energy conversion, storage, and release using an integrated solar-driven redox flow battery*¹ a single-crystal n-type WSe₂ is used in a 10 mM anthraquinone-2-sulfonate/iodide RFB. As was seen in reference,⁷ the cell voltage here is also lower than expected when we consider the actual RFB battery cycling tests. A value of 0.41 V can be evaluated when considering Figure 5b and taking the average of the potentials halfway through each charging and discharging curve.

$$E_{cell} = \frac{E_{charging,50} + E_{discharging,50}}{2} = \frac{0.48V + 0.33V}{2} = 0.405V$$

The same value can be read off from Figure 5c when reading of the open circuit potential at half charging and discharging time. The RFB capacity is thus calculated to 0.22 WhL⁻¹. Regarding solar charging the authors show photoelectrochemical characterization up to 0.39 V (their optimized value) in Figure 8, which translates to 34% SOC when using a cell potential of 0.405 V, and they calculate the solar conversion efficiency to 3.9%.

8) In the report *An All-vanadium Continuous-flow Photoelectrochemical Cell for Extending State-of-charge in Solar Energy Storage*⁸ the solar battery of ref² is revisited. The authors reach 21% SOC which is corroborated by voltage and UV measurements and they calculate solar conversion efficiency to be 0.6% assuming a 90 % efficient RFB, which we do not take into account here, so the value used in Figure 1 is 0.66%.

9) In the report *Photorechargeable High Voltage Redox Battery Enabled by Ta₃N₅ and GaN/Si Dual-Photoelectrode*⁹ a dual-semiconductor solar RFB is constructed from a Ta₃N₅ photoanode and a pn⁺Si/GaN/TiO₂ in a 0.4 M ferrocyanide/2,6-dihydroxyanthraquinone alkaline RFB with a cell potential of 1.2 V resulting in a RFB capacity of 6.43 WhL⁻¹. The authors show a full-cell linear sweep with unbiased current density of 0.93 mA cm⁻² in Figure 4b, however in the full photocharging test in the Supporting Information (S9) an initial (unstable) current of 0.5 mA at 0% SOC is only indicated without area specification. Halfway through this charging curve going to 22% SOC (calculated from capacity in Figure S9), the current has dropped to 0.4 mA (20% drop). Thus we can estimate that at 11% SOC at a battery voltage of 1.12 V the current density is 80% of 0.93 mA cm⁻² equal to 0.74 mA cm⁻² giving a solar conversion efficiency of 0.83%.

S2: TEMPO-sulfate: Attenuated Total Reflectance Fourier Transform Infrared Spectroscopy

Infrared spectra of the starting chemical (4-hydroxy-TEMPO, >99%) and the synthesis product was recorded on a Nicolet FT-IR Spectrometer (iS5, Thermo Fisher Scientific, USA) controlled with the OMNIC software (Thermo Fisher Scientific, USA). The background (ambient atmosphere) was subtracted from the recorded sample spectra. Assignment of selected peaks illustrating the chemical change of the compound from an alcohol to a sulfate are seen in Figure S1 below.

Secondary alkyl sulfate salts generally have a very strong doublet at 1270-1210 cm^{-1} and a strong band at 1075-1050 cm^{-1} which are due to symmetric and asymmetric stretching vibrations of the SO_2 group.¹⁰ A medium intensity band should be seen from 945-925 cm^{-1} as well, but is observed at 965 cm^{-1} . The S-O-C stretching vibrations are found around 875 cm^{-1} and 750 cm^{-1} , while SO_3 bending vibration should cause two medium-strong bands at 700-570 cm^{-1} . The band positions can be influenced from the tabulated values by the nature of the metal counter ion, which may explain slight deviations (here observed from a shift of the 750 cm^{-1} band to just below 800 cm^{-1}). Around 3500 cm^{-1} , the synthesis product shows two sharp peaks accompanied by a peak at 1640 cm^{-1} which can be assigned to OH-stretching of water of crystallization indicating that the compound is not completely dry.¹¹ The 4-hydroxy-TEMPO spectrum on the other hand shows a sharp peak at 3400 cm^{-1} coming from intramolecularly H-bonded O-H from the alcohol group.^{11,12} Stretching of the nitroxide group is seen at 1371 cm^{-1} for 4-hydroxy-TEMPO, but a variety of bands in the area 1400-1340 cm^{-1} obscures the clarity of this peak such as e.g. the C-H bending of CH_3 .^{11,12} The spectra confirms the expected change from an alcohol to a sulfate group, although no purity can be estimated.

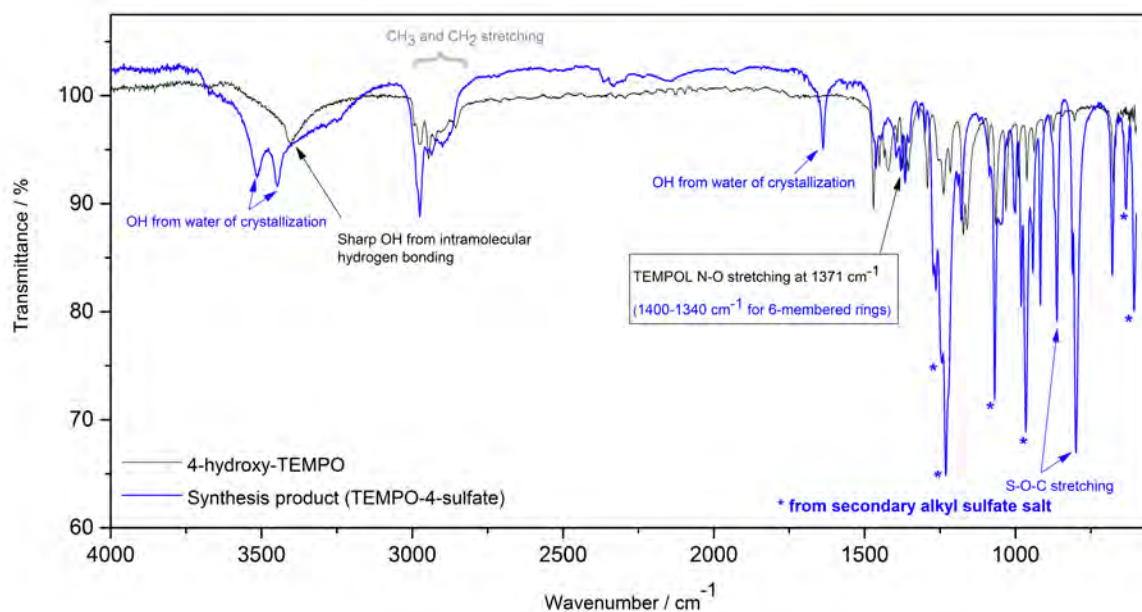


Figure S1: FT-IR spectrum recorded for 4-hydroxy-TEMPO (black) and the synthesis product (blue) used in battery tests.

S3: Photoelectrochemical redox flow battery cell

The photoelectrochemical flow cell is made from POM (polyoxymethylene) and shown in Figure S2 and features a 1 cm^2 quartz glass window. The photoelectrode is contacted from the front of the cell by gluing it to a plastic holder designed to fit inside the cell allowing for the (isolated) copper wire to come out at the front of the assembled piece, whereby it can be contacted to the brass rod photoelectrode contact of the cell. The two sides of the cell is sealed from each other by a membrane pressed against two o-rings and a 1 mm spacer. On the backside, a gold-plated copper current collector with a piece of graphite glued to it and pressed together with two heat-treated carbon papers, acts as the graphite anode (in the figure below only a copper plate can be seen). The flow is maintained through the cell by pumping through Viton tubing with a peristaltic pump (BT600L Zhengzhou Mingyi Instrument Equipment CO., LTD). The Viton is connected to the cell via PEEK fittings.

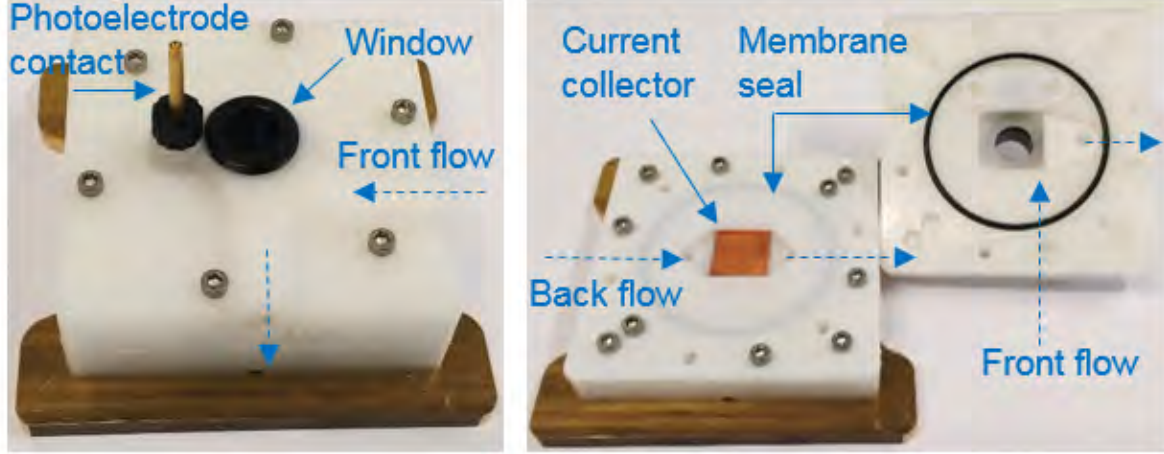
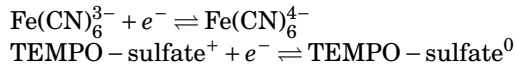


Figure S2: Photoelectrochemical flow cell showing the assembled cell and the inside front and back.

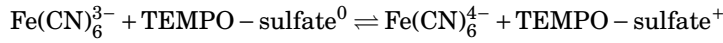
S4: Additional RFB data

Figure S3 shows the cell potential (U_{cell}) as a function of charging time for the first charging of the two experiments shown in Figure 3b and c in the main paper (green curves). These are plotted on top of a theoretical charging curve (blue curve) based on the Nernst equation and the redox potentials of the redox couples.

The redox reactions are:



So the overall cell reaction is:



The cell potential during charging is given by:

$$U_{cell} = U_{pol} + E_{cell}^0 + \frac{RT}{nF} \cdot \ln \left(\frac{[\text{TEMPO-sulfate}^+][\text{Fe(CN)}_6^{4-}]}{[\text{TEMPO-sulfate}^0][\text{Fe(CN)}_6^{3-}]} \right)$$

Here U_{pol} is the polarization overpotential due to the charging, E_{cell}^0 is the standard cell potential and $n = 1$ electron. The rest is the Nernstian contribution to the cell potential.

Assuming equal starting concentrations (0.4 M in all tests) of Fe(CN)_6^{3-} and TEMPO-sulfate^0 , and using the definition of SOC:

$$\text{SOC}\% = \frac{[\text{Fe(CN)}_6^{4-}]}{[\text{Fe(CN)}_6^{3-}] + [\text{Fe(CN)}_6^{4-}]} \cdot 100\% = \frac{[\text{TEMPO-sulfate}^+]}{[\text{TEMPO-sulfate}^0] + [\text{TEMPO-sulfate}^+]} \cdot 100\%$$

the cell potential and SOC is related by:

$$U_{cell} = U_{pol} + E_{cell}^0 + \frac{RT}{nF} \cdot \ln \left(\frac{\text{SOC}^2}{(1-\text{SOC})^2} \right)$$

The cell area resistance in the current setup is around $1.2 \Omega \text{ cm}^2$ and with current densities below 12.5 mA cm^{-2} the maximum U_{pol} is estimated to be around 15 mV and small compared to other contributions. In Figure S3 a good agreement between the theoretical cell potential (with $U_{pol} = 0$) and the observed charging potential curve is seen (with $E_{cell}^0 = 0.35 \text{ V}$ as determined from the CVs in Figure 3a of the main paper). These experiments gives confidence that the SOC can be determined from open-circuited potential (U_{OCV}) measurements of the electrolytes. Throughout the paper the SOC is determined from measurements of U_{OCV} using the equation:

$$U_{\text{cell}} = E_{\text{cell}}^0 + \frac{RT}{F} \cdot \ln\left(\frac{\text{SOC}^2}{(1-\text{SOC})^2}\right)$$

with $E_{\text{cell}}^0 = 0.35 \text{ V}$.

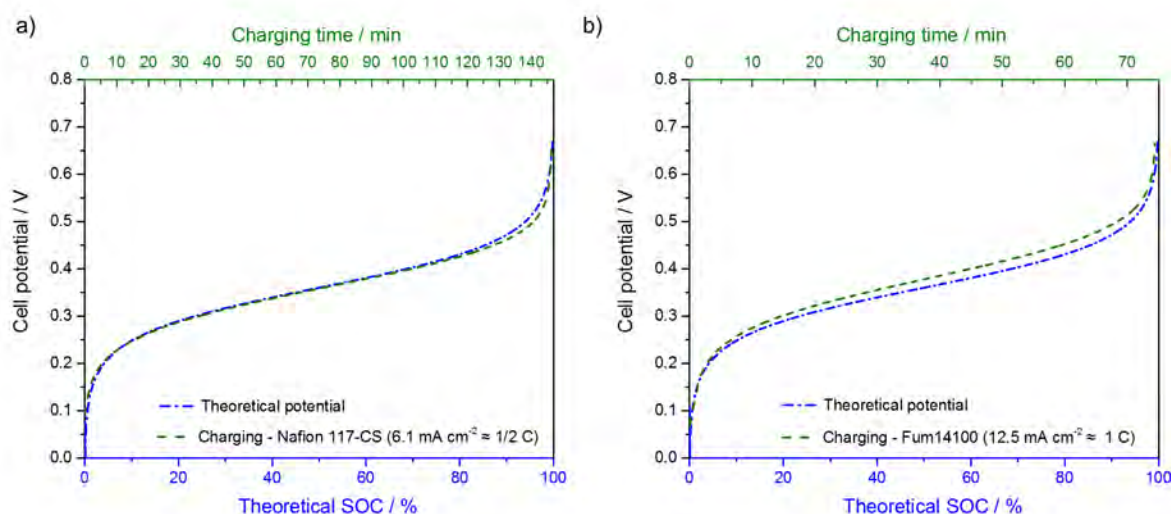


Figure S3: The theoretical cell voltage of the battery as a function of the state-of-charge calculated from the Nernst equation (blue curve) plotted against the observed charging curves in case of a) the battery test with Nafion and b) the battery test with Fumasep14100.

Post-battery cycling CVs were recorded as described in the Experimental Section of the main paper in a mixture of 0.1 mL of battery electrolyte mixed in 20 mL 1 M NH₄Cl at pH 7. They are shown in Figure S4 after 12 battery cycles with a Nafion membrane (Figure S4a) showing extensive crossover and after 135 cycles with Fumasep14100 (Figure S4b) showing less crossover.

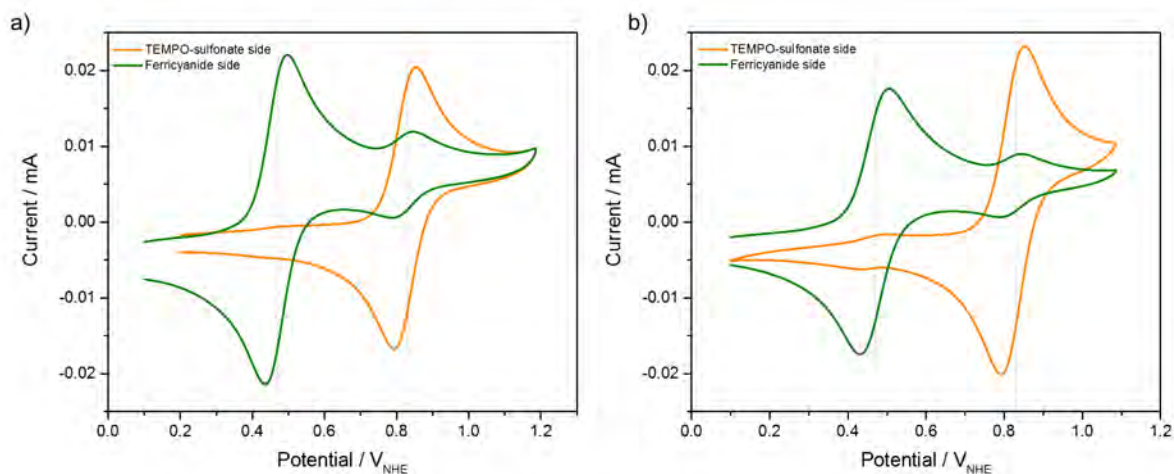


Figure S4: Post-battery cycling CVs at a scan rate of 0.1 V s⁻¹ a) after the 12 cycles with Nafion and b) after 135 cycles with Fumasep14100.

Pictures of the blue coloration of the membranes were taken immediately after cycling and are shown in Figure S5.

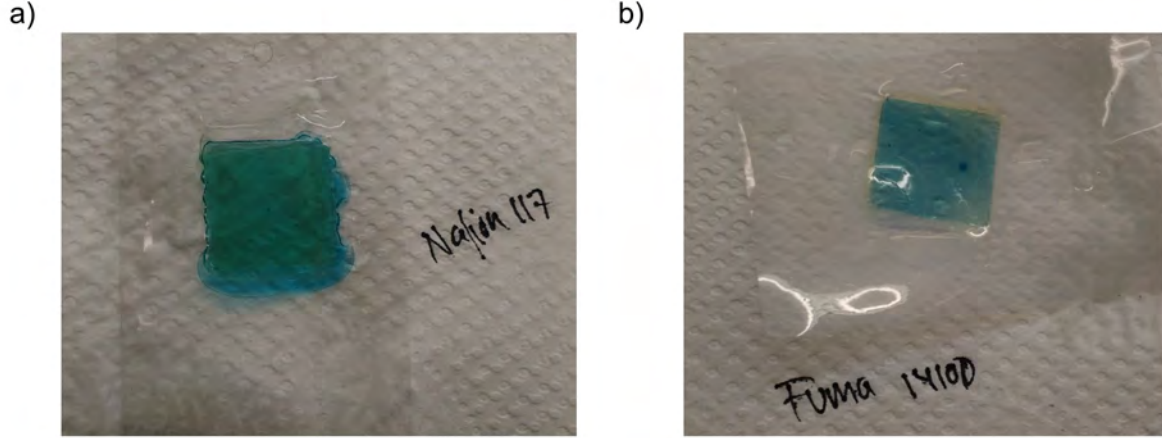


Figure S5: Post-battery cycling membrane colouration of a) Nafion after 12 cycles and b) Fumasep14100 after 135 cycles.

S5: Photoelectrode energy levels (Figure 4)

The photoelectrode band diagram has been explored in past works where the electrode was used for photocathodic hydrogen production.¹³⁻¹⁶ The p-Si wafer has band gap of 1.124 V. If we consider first the p-n⁺-Si junction, there will be an internal band bending, which results in a consistent photovoltage regardless of electrolyte interactions.¹⁷ This built-in potential can be calculated by:

$$V_{\text{built-in}} = \frac{kT}{e} \ln \left(\frac{N_{D,n-Si} \cdot N_{A,p-Si}}{n_i^2} \right)$$

where the donor density of the n⁺-Si, $N_{D,n-Si}$, is $5 \cdot 10^{19} \text{ cm}^{-3}$, the acceptor density of p-Si, $N_{A,p-Si}$, is $3 \cdot 10^{15} \text{ cm}^{-3}$ and n_i is the intrinsic carrier density of Si with a value of $1.5 \cdot 10^{10} \text{ cm}^{-3}$. These values result in a built-in potential of 0.88 V.

The depletion width can then be calculated:

$$W = \sqrt{\frac{2\epsilon_0\epsilon_{Si}(N_{D,n-Si} + N_{A,p-Si})V_{\text{built-in}}}{e \cdot N_{D,n-Si} \cdot N_{A,p-Si}}}$$

where ϵ_0 is the permittivity in vacuum and ϵ_{Si} is the relative permittivity of Si and equal to 11.7. This calculation results in a depletion width of 615 nm, and the distribution of this between the p-Si and n⁺-Si can be calculated as well:

$$x_{p-Si} = \frac{N_{D,n-Si}}{N_{A,p-Si} + N_{D,n-Si}} \cdot W$$

$$x_{n-Si} = \frac{N_{A,p-Si}}{N_{A,p-Si} + N_{D,n-Si}} \cdot W$$

which results in a depletion almost completely in the p-Si layer.

Considering next the Ti layer, the function is to prevent silicon oxidation under the reactive sputtering conditions when depositing TiO₂. The layer could be assumed to be an ohmic contact or a Schottky barrier. In the case it is an ohmic contact, there will be no potential distribution across it, but if it is a Schottky barrier with no metal-induced gap states or Fermi level pinning, there will be a barrier height determined by:

$$\Phi_{Bi,Si} = \Phi_{Ti} - \Phi_{Si} + \frac{kT}{e} \ln \left(\frac{N_{C,Si}}{N_{D,n-Si}} \right)$$

where $\Phi_{Bi,Si}$ is the work function of Ti equal to 4.33 V and Φ_{Si} is used instead of Φ_{n^+-Si} , which is assumed to be close to the electron affinity of Si equal to 4.15 V corrected for the difference between flat band and conduction band using a n⁺ donor density value, $N_{C,Si}$ of $2.8 \cdot 10^{15} \text{ cm}^{-3}$.¹⁸ The barrier height is thus 0.072

V and the barrier width is then given by:

$$W = \sqrt{\frac{2\epsilon_0\epsilon_{Si}\Phi_{Bi,Si}}{e\cdot N_{D,n-Si}}}$$

resulting in a width of 1.36 nm, which is a distance small enough to allow electrons to transfer from n⁺-Si to Ti through tunnelling.

The metallic Pt layer on the outer surface should be fixed at the redox potential of the electrolyte that it is in contact with. If we assume that it is a Schottky barrier with no metal induced gaps states and Fermi level pinning (reasonable for a flat Pt coverage with no pinholes) the built-in potential barrier height is:

$$\Phi_{Bi,TiO_2} = \Phi_B - \frac{kT}{e} \ln\left(\frac{N_{C,TiO_2}}{N_{D,TiO_2}}\right)$$

where N_{C,TiO_2} is the density of state of TiO₂ in the conduction band and equal to $7.86\cdot 10^{20}$ cm⁻³ and N_{D,TiO_2} is the donor density of the TiO₂ which can be determined by Mott-Schottky analysis (see below).¹⁹ Φ_B is the barrier height determined by:

$$\Phi_B = \Phi_{Pt} - \chi_{TiO_2}$$

where Φ_{Pt} is the work function of Pt equal to 5.08 eV and χ_{TiO_2} is the electron affinity of TiO₂ identical to the conduction band position, E_{CB} , of the TiO₂, which can also be determined from Mott-Schottky analysis.²⁰ The depletion width can be calculated as for the Ti/n⁺ layer.

Mott-Schottky analysis was done in the dark using the built-in function of the CHI660E potentiostat in an electrochemical cell consisting of a platinum wire counter electrode, a Ag/AgCl (sat) reference electrode and a Ti/TiO₂ covered n⁺-Si working electrode with or without Pt on top. The potential was changed in increments of 10 mV, and an amplitude of 10 mV was used at a frequency of 100 Hz. The donor density was determined from the Mott-Schottky equation:

$$\frac{1}{C^2} = \frac{2}{q\epsilon_{TiO_2}\epsilon_0 A N_{D,TiO_2}} \left(E - E_{FB} - \frac{kT}{e} \right)$$

where C is the capacity, ϵ_{TiO_2} is the relative permittivity of TiO₂ (here we use a value for anatase of 36, A is the electrode area and E_{FB} is the flatband potential.^{21,22} The conduction band position can be calculated by:

$$E_{CB} = E_{FB} - \frac{kT}{e} \ln\left(\frac{N_{D,TiO_2}}{N_{C,TiO_2}}\right)$$

Figure S6 below shows recorded Mott-Schottky spectra in different electrolytes, with and without Pt as well as the calculated barrier height (0.6-0.8 V) and depletion width. The depletion width is on the order of magnitude small enough for electrons to tunnel through.²³

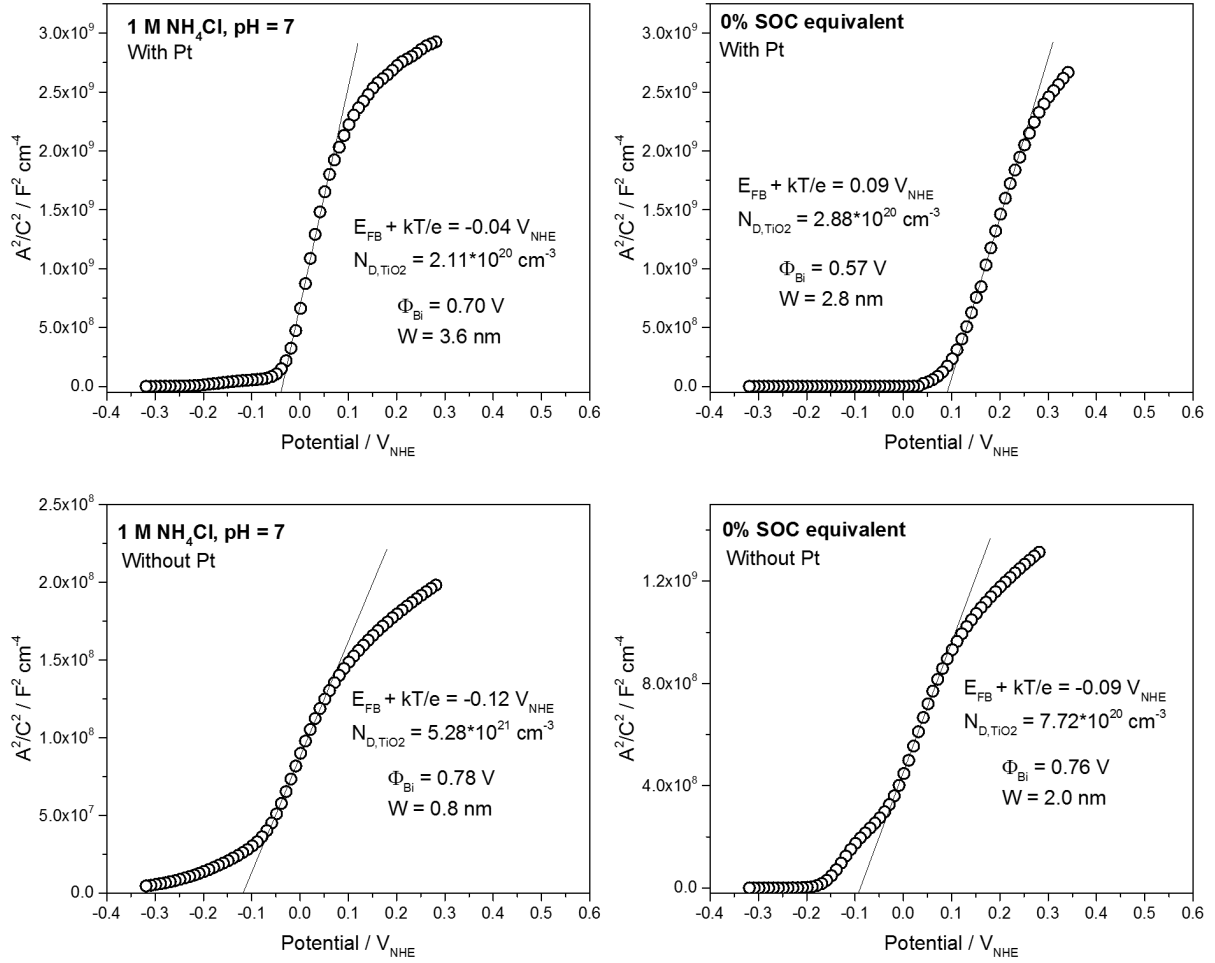


Figure S6: Mott-Schottky spectra and derived quantities.

In order to draw the energy diagram at different SOC's i.e. at different working potentials, the valence band position of the p-Si was determined as a function of the working potential E by:

$$E_{VB,p-Si} = E - \frac{kT}{e} \ln \left(\frac{N_{A,p-Si}}{N_{V,Si}} \right)$$

where $N_{V,Si}$ is the density of states in the valence band and equal to $1.8 \cdot 10^{19} \text{ cm}^{-3}$. E is taken as the ferri/ferrocyanide redox potential at different SOC's calculated from the Nernst equation to be $0.651 V_{NHE}$, $0.475 V_{NHE}$ and $0.400 V_{NHE}$ for 0%, 50% and 95% SOC, respectively. This results in corresponding valence band positions of $0.873 V_{NHE}$, $0.699 V_{NHE}$ and $0.624 V_{NHE}$. From these positions, the photovoltage of $0.515 V$ determined from Figure 3a of the main paper and calculated depletion widths, the band diagram can be constructed for each case. In Figure S7 is shown the 0%, 50% and 95% SOC band diagrams. It is seen that the most driving force for the unbiased electrochemical process is found in the 0% SOC case (largest potential drop for the h^+ to the TEMPO-sulfate redox potential), while the lowest is found in the 95% SOC case as would be expected.

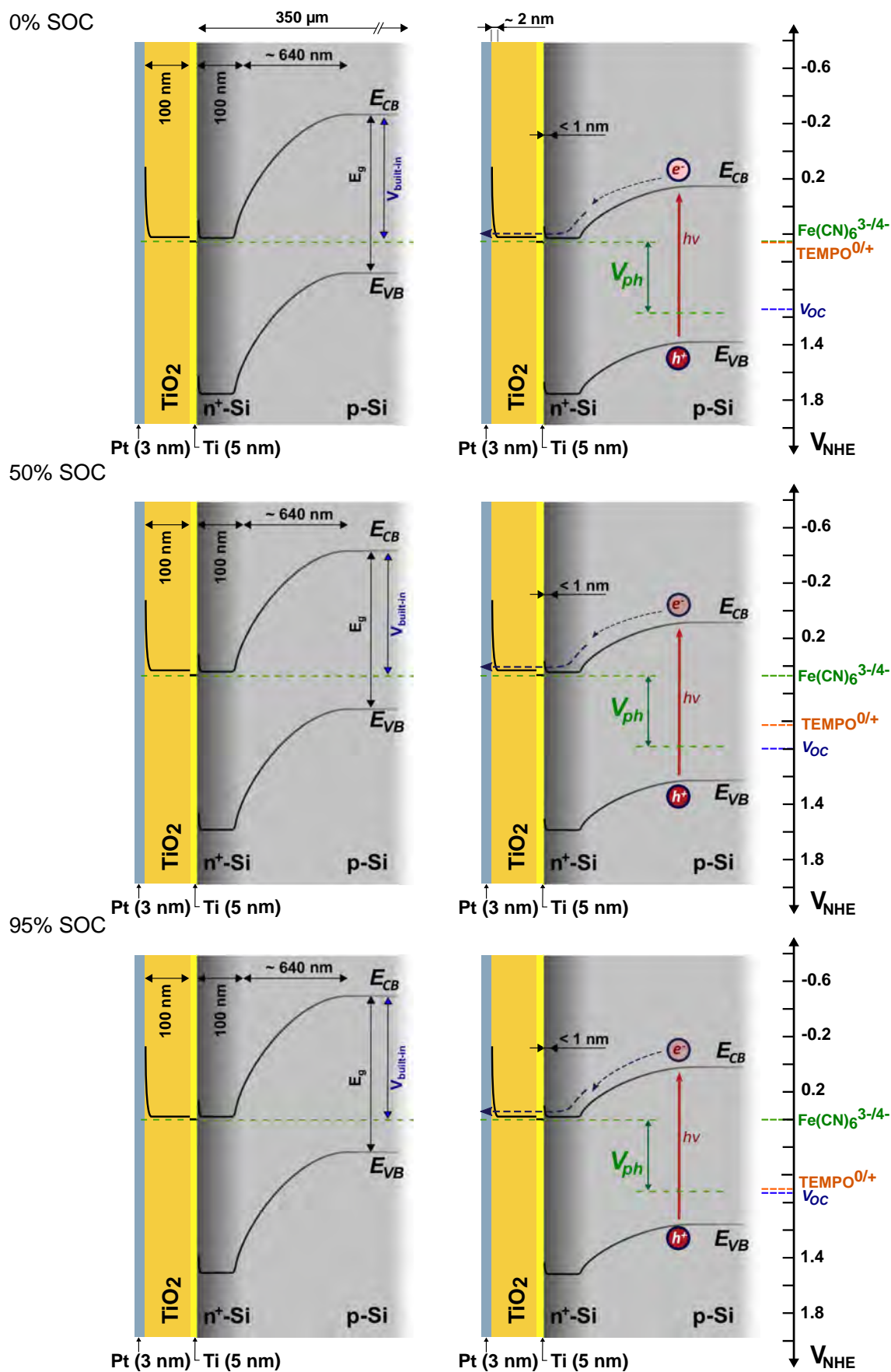


Figure S7: Band diagrams for 0%, 50% and 95% SOC (where the working potential of the system is set at the redox potential of the ferri/ferrocyanide solution) in the dark and in the light. The blue dotted lines denote the measured open-circuit potentials in the light, the green dotted line the ferri/ferrocyanide redox potential and orange dotted line the TEMPO-sulfate redox potential at the given SOC.

S6: Photocathode water splitting performance

The photocathode water splitting performance was evaluated by recording LSVs in the same 3-electrode cell as used for Figure 5 in the main paper in the dark and light (AM 1.5G). The solution resistance remained uncompensated. The voltage range from photocurrent onset and until a stable photocurrent is reached is indicated in Figure S8 and increases significantly with the pH being above 500 mV in the case of neutral 1 M KCl solution. The early onset (0.6 V_{RHE}) in the case of 1 M NH₄Cl has been observed earlier and can be explained by dissolved molecular hydrogen in the solution close to the electrode surface or (here less likely) hydrogen bubbles trapped at the surface.²⁴ Noticeably, these highly reductive potential ranges are out of the expected working range for a solar battery and reported relatively to the Reversible Hydrogen Electrode (RH) rather than the Normal Hydrogen Electrode for comparison of the performance at different pH.

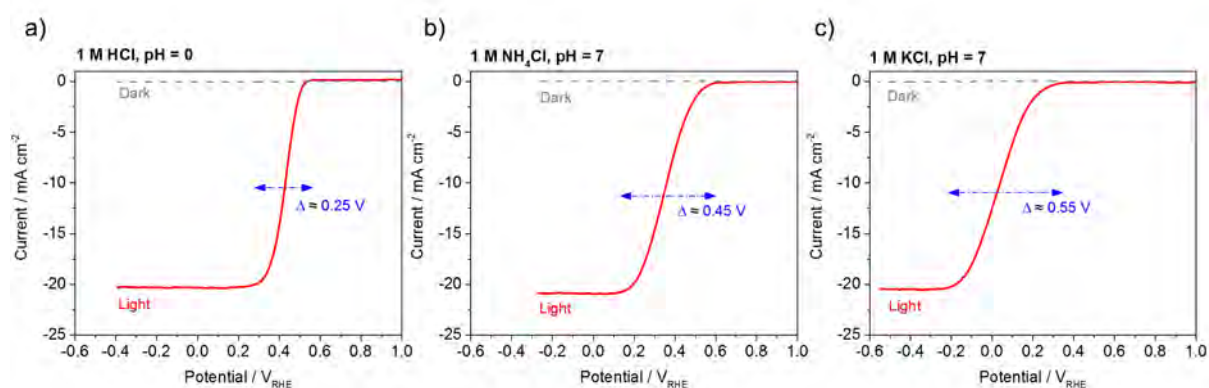


Figure S8: LSVs recorded in a 3-electrode cell (working electrode pn^+Si/TiO_2 , Ag/AgCl reference electrode and Pt counter electrode) in the dark and in the light (resistance uncompensated) in a) 1 M HCl, b) 1 M NH₄Cl and c) 1 M KCl. For b) and c) the pH of the solution was adjusted to 7.

S7: Photoelectrode and solution transmittance

To determine the optical loss by TiO_2 and Pt thin films, optical transmission measurements were performed using a Varian Cary 1E UV-VIS spectrophotometer. Pyrex glass substrates have been used for this UV-Vis measurement and the protection layers were deposited as described in the main paper. The band gap of TiO_2 (anatase) is 3.2 eV which converted to wavelength is 387 nm, below which the transmittance is very limited as seen in Figure S9.²⁰ The Ti/ TiO_2 layer shows an unconventionally low transmittance compared to that from previous studies, which might be due to the remaining Ti interlayer which is not fully converted to TiO_2 . Addition of 3 nm metallic Pt catalytic layer leads to further decrease in transmittance.

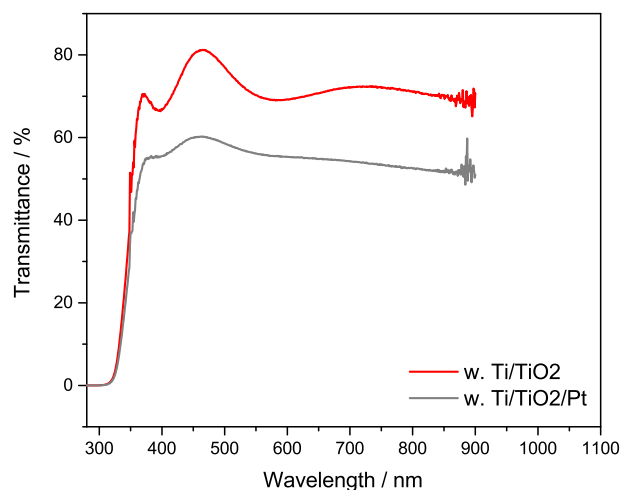


Figure S9: Transmittance of the top Ti/ TiO_2 and Ti/ TiO_2 /Pt layers deposited on a glass substrates.

From the measured absorbance of the diluted SOC equivalent solutions shown in Figure 5b of the main paper, the full absorbance and transmittance (Figure S10c) through 2 mm and 1 mm electrolyte was determined from the extinction coefficient calculated at individual wavelengths from 300-480 nm by using Lambert Beer's law. The extinction coefficient at 420 nm is $1056 \text{ L mol}^{-1} \text{ cm}^{-1}$ which compares well to literature values.^{25,26} The correlation coefficient for the linear regression to get the extinction coefficient is close to 1 around the peaks in the area of interest as shown in Figure S10b. Figure S10c shows the combined transmittance spectra of the solution and protection layers and it is clear that from ca. 430 nm and downwards, the transmittance is very limited.

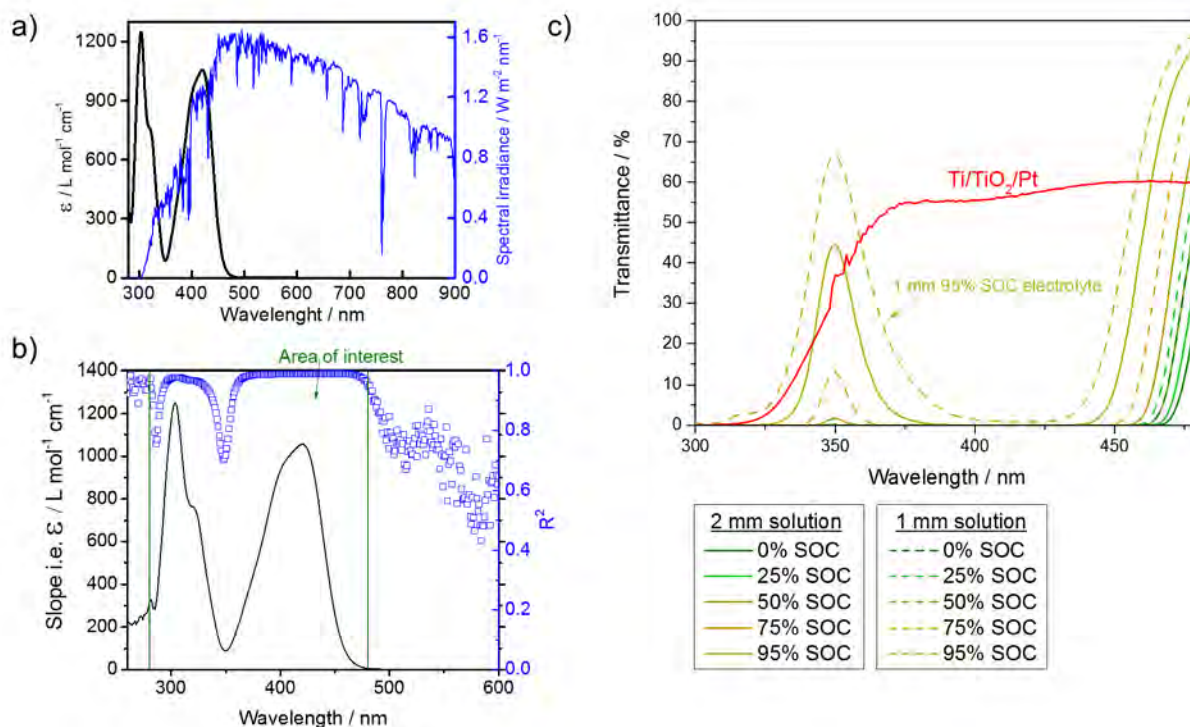


Figure S10: a) Zoom of the inset in Figure 5b of the main paper showing the calculated extinction coefficients overlaid on the AM1.5G spectrum.²⁷ b) The same extinction coefficients (slopes) from the linear regression and the correlation coefficient of the fit. c) The calculated transmittance of 2 and 1 mm SOC equivalent solutions.

S8: Batch solar RFB test

In a solar RFB batch cell (described elsewhere⁵) that allows the use of both a photoelectrode and a graphite working electrode on the front side, assembled with the Fumasep14100 membrane, a $\text{pn}^+\text{Si}/\text{TiO}_2$ was used to record LSV curves using 25 mL 0.4 M electrolytes on each side. The electrolytes were brought to the indicated SOC in the batch photo cell on graphite electrodes and the SOC evaluated by a 15 min measurement of the open-circuit potential after manual electrolyte stirring in each chamber. A selection of LSVs are shown in Figure S11.

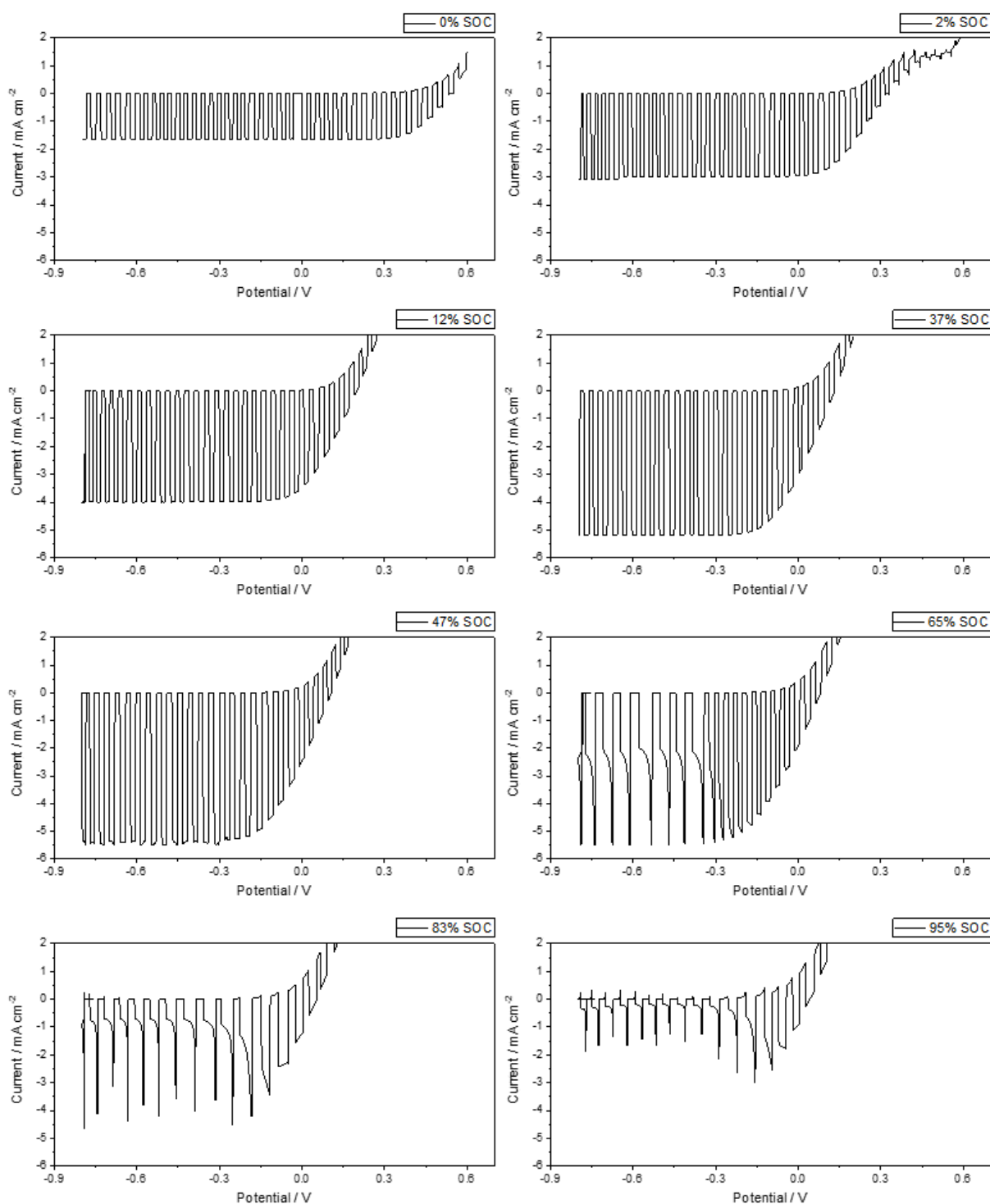


Figure S11: Linear sweep voltammetry on pn^+Si/TiO_2 in the photoelectrochemical batch battery cell ($0.4 M$ electrolytes at different SOC) using a Fumasep14100 membrane.

S9: Solar RFB photocharging test

In the photoelectrochemical flow cell, a test of 3 hours uninterrupted illumination (no voltage bias) resulted in the time-SOC curve shown in Figure S12a. LSVs were recorded in the beginning (0% SOC) and after 40, 50, 110 and 130 min of photocharging time and the SOC was evaluated from an established correlation between onset potential on the photoelectrode and the battery SOC as measured on graphite seen in Figure S12.

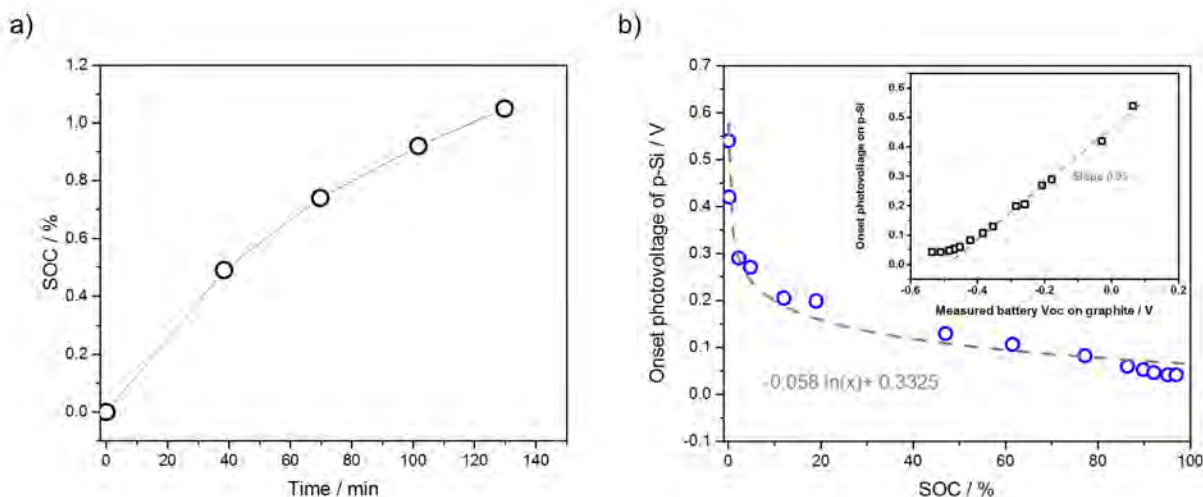


Figure S12: a) Increase in the SOC upon 140 min unbiased 1 sun illumination. The SOC is determined from an established correlation b) between the full cell voltage measured on graphite and the photocathode onset potential.

The photocharging test could not be continued, as the membrane clogged with a red precipitate (supposedly Fe_2O_3) and increased the cell resistance very much. A photo of the cell after the phototest is seen in Figure S13.

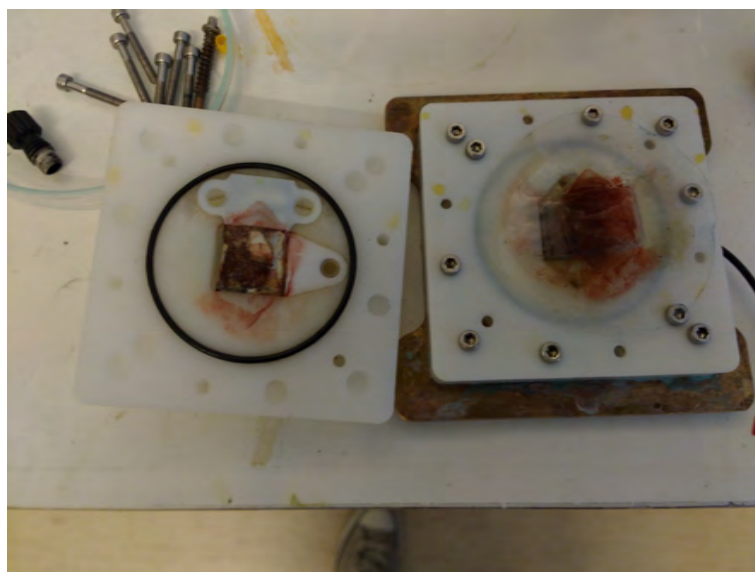


Figure S13: Red precipitate (supposedly Fe_2O_3) inside the photoelectrochemical flow cell after prolonged illumination (3 hours).

S10: Photoelectrode stability test

A photoelectrode was subjected to a longer interrupted illumination in a 0% SOC equivalent solution in a 3-electrode setup in order to determine the time scale of its stability. A potential of $0.4 \text{ V}_{\text{NHE}}$ was applied, and the sample left under 1 sun illumination for 1 hour intervals interrupted by 1 hour in the dark. The resulting photocurrent is seen in Figure S14. After 8 hours light/dark the solution was changed to a fresh one. It is seen that the photocurrent drops with time, but that the introduction of fresh electrolyte restores (even improves) the photocurrent which indicates that degradation is caused mainly by the ferricyanide

light instability and to a lesser extent photoelectrode corrosion. A red precipitate was observed in the test, while the absorbance of the illuminated solution remained unchanged from that of the fresh one, which would be expected, as iron oxide is insoluble at neutral pH.

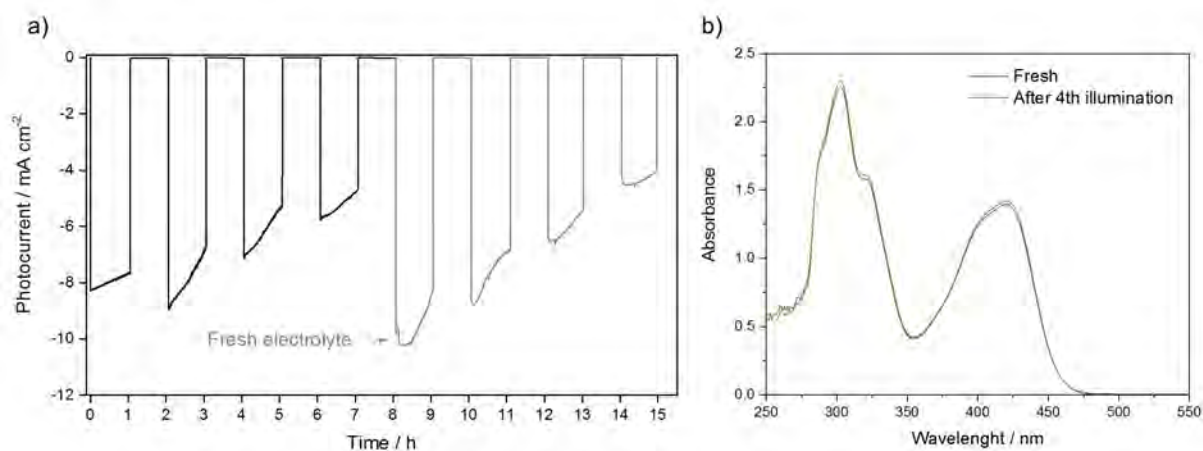


Figure S14: a) Photocurrent when subjecting a photoelectrode to 1 hour light/dark intervals and b) absorbance (diluted 300 times) of the used solution fresh and after 8 hours.

References

- [1] J. R. McKone, F. J. DiSalvo, and H. D. Abruña, "Solar energy conversion, storage, and release using an integrated solar-driven redox flow battery," *Journal of Materials Chemistry A*, vol. 5, pp. 5362–5372, Mar. 2017.
- [2] Z. Wei, D. Liu, C. Hsu, and F. Liu, "All-vanadium redox photoelectrochemical cell: An approach to store solar energy," *Electrochemistry Communications*, vol. 45, pp. 79–82, Aug. 2014.
- [3] J. Azevedo, T. Seipp, J. Burfeind, C. Sousa, A. Bentien, J. P. Araújo, and A. Mendes, "Unbiased solar energy storage: Photoelectrochemical redox flow battery," *Nano Energy*, vol. 22, pp. 396–405, Apr. 2016.
- [4] M. Yu, X. Ren, L. Ma, and Y. Wu, "Integrating a redox-coupled dye-sensitized photoelectrode into a lithium–oxygen battery for photoassisted charging," *Nature Communications*, vol. 5, p. 5111, Oct. 2014.
- [5] K. Wedege, J. Azevedo, A. Khataee, A. Bentien, and A. Mendes, "Direct Solar Charging of an Organic–Inorganic, Stable, and Aqueous Alkaline Redox Flow Battery with a Hematite Photoanode," *Angewandte Chemie International Edition*, vol. 55, pp. 7142–7147, June 2016.
- [6] W. D. McCulloch, M. Yu, and Y. Wu, "pH-Tuning a Solar Redox Flow Battery for Integrated Energy Conversion and Storage," *ACS Energy Letters*, vol. 1, pp. 578–582, Sept. 2016.
- [7] W. Li, H.-C. Fu, L. Li, M. Cabán-Acevedo, J.-H. He, and S. Jin, "Integrated Photoelectrochemical Solar Energy Conversion and Organic Redox Flow Battery Devices," *Angewandte Chemie International Edition*, vol. 55, pp. 13104–13108, Oct. 2016.
- [8] Z. Wei, Y. Shen, D. Liu, and F. Liu, "An All-vanadium Continuous-flow Photoelectrochemical Cell for Extending State-of-charge in Solar Energy Storage," *Scientific Reports*, vol. 7, p. 629, Apr. 2017.
- [9] Q. Cheng, W. Fan, Y. He, P. Ma, S. Vanka, S. Fan, Z. Mi, and D. Wang, "Photorechargeable High Voltage Redox Battery Enabled by Ta₃N₅ and GaN/Si Dual-Photoelectrode," *Advanced Materials*, vol. 29, no. 26, p. 1700312, 2017.
- [10] D. A. Long, "Infrared and Raman characteristic group frequencies. Tables and charts George Socrates John Wiley and Sons, Ltd, Chichester.," *Journal of Raman Spectroscopy*, vol. 35, pp. 905–905, Oct. 2004.
- [11] D. H. Williams and I. Fleming, *Spectroscopic Methods in Organic Chemistry*. London: McGraw-Hill Education, 6th edition ed., Dec. 2007.
- [12] P. Franchi, M. Lucarini, P. Pedrielli, and G. F. Pedulli, "Nitroxide Radicals as Hydrogen Bonding Acceptors. An Infrared and EPR Study," *ChemPhysChem*, vol. 3, pp. 789–793, Sept. 2002.
- [13] B. Seger, T. Pedersen, A. B. Laursen, P. C. K. Vesborg, O. Hansen, and I. Chorkendorff, "Using TiO₂ as a Conductive Protective Layer for Photocathodic H₂ Evolution," *Journal of the American Chemical Society*, vol. 135, pp. 1057–1064, Jan. 2013.
- [14] D. Bae, S. Shayestehaminzadeh, E. B. Thorsteinsson, T. Pedersen, O. Hansen, B. Seger, P. C. K. Vesborg, S. Ólafsson, and I. Chorkendorff, "Protection of Si photocathode using TiO₂ deposited by high power impulse magnetron sputtering for H₂ evolution in alkaline media," *Solar Energy Materials and Solar Cells*, vol. 144, pp. 758–765, Jan. 2016.
- [15] D. Bae, B. Seger, P. C. K. Vesborg, O. Hansen, and I. Chorkendorff, "Strategies for stable water splitting via protected photoelectrodes," *Chemical Society Reviews*, vol. 46, pp. 1933–1954, Apr. 2017.
- [16] Bart Van Zeghbroeck, "Principles of Electronic Devices," 2011.
- [17] E. L. Warren, S. W. Boettcher, M. G. Walter, H. A. Atwater, and N. S. Lewis, "pH-Independent, 520 mV Open-Circuit Voltages of Si/Methyl Viologen^{2+/+} Contacts Through Use of Radial n+p-Si Junction Microwire Array Photoelectrodes," *The Journal of Physical Chemistry C*, vol. 115, pp. 594–598, Jan. 2011.

- [18] D. Bae, B. Mei, R. Frydendal, T. Pedersen, B. Seger, O. Hansen, P. C. K. Vesborg, and I. Chorkendorff, "Back-Illuminated Si-Based Photoanode with Nickel Cobalt Oxide Catalytic Protection Layer," *Chem-ElectroChem*, vol. 3, pp. 1546–1552, Oct. 2016.
- [19] I. A. Digdaya, L. Han, T. W. F. Buijs, M. Zeman, B. Dam, A. H. M. Smets, and W. A. Smith, "Extracting large photovoltages from a-SiC photocathodes with an amorphous TiO₂ front surface field layer for solar hydrogen evolution," *Energy & Environmental Science*, vol. 8, no. 5, pp. 1585–1593, 2015.
- [20] W. M. Haynes, *CRC Handbook of Chemistry and Physics, 93rd Edition*. CRC Press, Apr. 2016.
- [21] I. Oja, A. Mere, M. Krunkk, R. Nisumaa, C. H. Solterbeck, and M. Es-Souni, "Structural and electrical characterization of TiO₂ films grown by spray pyrolysis," *Thin Solid Films*, vol. 515, pp. 674–677, Oct. 2006.
- [22] S. K. Kim, W.-D. Kim, K.-M. Kim, C. S. Hwang, and J. Jeong, "High dielectric constant TiO₂ thin films on a Ru electrode grown at 250 °C by atomic-layer deposition," *Applied Physics Letters*, vol. 85, pp. 4112–4114, Nov. 2004.
- [23] R. G. Lerner and G. L. Trigg, *Encyclopedia of Physics, 2 Volumes*. Dec. 2005.
- [24] O. Berkh, Y. Shacham-Diamand, and E. Gileadi, "Reduction of Ammonium Ion on Pt Electrodes," *Journal of The Electrochemical Society*, vol. 155, pp. F223–F229, Oct. 2008.
- [25] M. Chakrabarti and E. Roberts, "Analysis of Mixtures of Ferrocyanide and Ferricyanide using UV-Visible Spectroscopy for Characterisation of a Novel Redox Flow Battery," *Journal of The Chemical Society of Pakistan*, vol. 30, no. 6, pp. 817–823, 2008.
- [26] S. Aldrich, "Potassium hexacyanoferrate(III) ASC Reagent Product Information."
- [27] A. S. F. Testing and Materials, *ASTM G173-03 Terrestrial (AM1.5) Reference Spectra*. 2003.